Article

Prototypal Dithiazolodithiazolyl Radicals: Synthesis, Structures, and Transport Properties

Leanne Beer, James F. Britten, Jaclyn L. Brusso, A. Wallace Cordes, Robert C. Haddon, Mikhail E. Itkis, Douglas S. MacGregor, Richard T. Oakley, Robert W. Reed, and Craig M. Robertson

J. Am. Chem. Soc., **2003**, 125 (47), 14394-14403• DOI: 10.1021/ja0371350 • Publication Date (Web): 04 November 2003

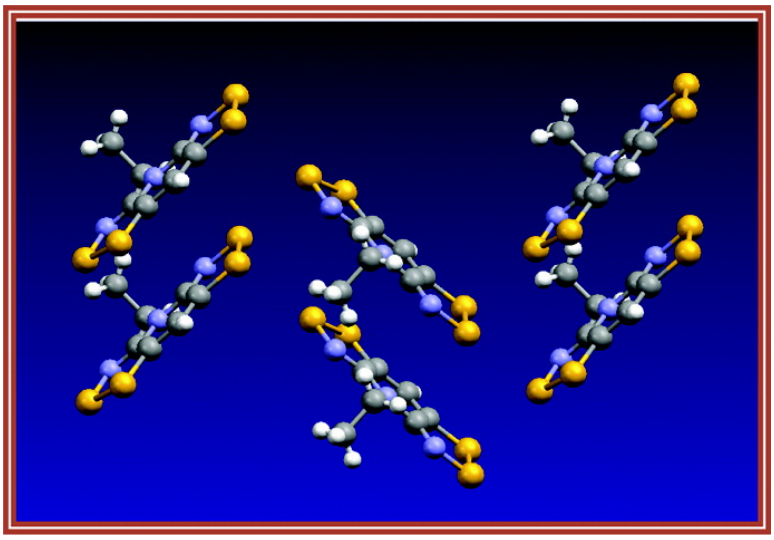

J|A|C|S
ARTICLES
Published on Web 11/04/2003

Prototypal Dithiazolodithiazolyl Radicals: Synthesis, Structures, and Transport Properties

Leanne Beer,[1a] James F. Britten,[1b] Jaclyn L. Brusso,[1a] A. Wallace Cordes,[1c] Robert C. Haddon,[1d] Mikhail E. Itkis,[1d] Douglas S. MacGregor,[1a] Richard T. Oakley,*[,1a] Robert W. Reed,[1a] and Craig M. Robertson[1a]

Contribution from the Department of Chemistry, University of Waterloo, Waterloo, Ontario N2L 3G1, Canada, Department of Chemistry, McMaster University, Hamilton, Ontario L8S 4M1, Canada, Department of Chemistry and Biochemistry, University of Arkansas, Fayetteville, Arkansas 72701, and Department of Chemistry and Center for Nanoscale Science and Engineering, University of California, Riverside, California 92521-0403

Received July 8, 2003; E-mail: oakley@sciborg.uwaterloo.ca

Abstract: New synthetic routes to 1,2,3-dithiazolo-1,2,3-dithiazolylium salts, based on double Herz condensations of N-alkylated 2,6-diaminopyridinium salts with sulfur monochloride, have been developed. The two prototypal 1,2,3-dithiazolo-1,2,3-dithiazolyl radicals HBPMe and HBPEt have been prepared and characterized in solution by cyclic voltammetry and EPR spectroscopy. Measured electrochemical cell potentials and computed (B3LYP/6-31G**) gas-phase disproportionation enthalpies favor a low on-site Coulombic repulsion energy U in the solid state. The crystal structures of HBPR (R = Me, Et) have been determined by X-ray crystallography (at 293 K). Both consist of slipped π-stacks of undimerized radicals, with many close intermolecular S- - -S contacts. Magnetic, conductivity, and optical measurements have been perfomed and the results interpreted in light of extended Hückel band calculations. The crystalline materials are paramagnetic above 100 K, with room-temperature conductivities σ_{RT} of 10^{-5}–10^{-6} S cm^{-1}; the slightly greater conductivity of the R = Et compound can be associated with a more well developed band structure. We suggest a Mott–Hubbard insulator ground state for these materials, with an on-site Coulomb repulsion energy U of about 1.0 eV.

Introduction

Single-component molecular conductors based on neutral π-radical building blocks represent an appealing alternative to conventional synthetic conductors,[2] which require charge transfer between two components[3] as a means of generating charge carriers. In an ideal neutral radical conductor, the unpaired electrons serve as charge carriers, and orbital overlap between adjacent radicals generates a half-filled energy band, as in an elemental metal such as sodium.[4] There are, however, two major problems associated with this model. First, a half-filled 1-D energy band is prone to a Peierls instability;[5] i.e., the radicals will dimerize. Second, if association can be suppressed, typically by steric bulk, the resulting low bandwidth W, coupled with the high on-site Coulomb repulsion energy U, leads to a Mott insulating state.[6] Insofar as U reaches a maximum for systems with a half-filled band ($f = {}^1/_2$), the need to control this parameter for neutral radical conductors is critical. We have therefore pursued the development of stable heterocyclic π-radicals in which U is minimized. To this end, we have sought materials with low gas-phase disproportionation enthalpies ΔH_{disp} (= IP − EA) and solution cell potentials E_{cell},[7] as these serve as guides to trends in U.[8−10] In addition, we have tried to design radicals that do not dimerize in the solid state and yet exhibit a strong network of intermolecular interactions, so that sufficient electronic bandwidth W is generated to offset U.

Within this context, the resonance-stabilized dithiazolodithiazolyl framework R_2BPR_1 **1** (Chart 1) represents an appealing system, conforming to both the energetic and structural criteria noted above. Recently, we reported the synthesis and structural

(1) (a) University of Waterloo. (b) McMaster University. (c) University of Arkansas. (d) University of California.
(2) (a) Marsitzky, D.; Mullen, K. In *Advances in Synthetic Metals*; Bernier, P., Lefrant, S., Bidan, G., Eds.; Elsevier: New York, 1999; p 1. (b) Grossel, M. C.; Weston, S. C. *Contemp. Org. Synth.* **1994**, *1*, 317. (c) Williams, J. M.; Ferraro, J. R.; Thorn, R. J.; Carlson, K. D.; Geiser, U.; Wang, H. U.; Kini, A. M.; Whangbo, M.-H. *Organic Superconductors (Including Fullerenes)*; Prentice Hall: Upper Saddle River, NJ, 1992. (d) Ferraro, J. R.; Williams, J. M. In *Introduction to Synthetic Electrical Conductors*; Academic Press: New York, 1987; p 25.
(3) Both components can, however, be incorporated into a single molecule. See, for example: Tanaka, H.; Okano, Y.; Kobayashi, H.; Suzuki, W.; Kobayashi, A. *Science* **2001**, *291*, 281.
(4) (a) Haddon, R. C. *Nature* **1975**, *256*, 394. (b) Haddon, R. C. *Aust. J. Chem.* **1975**, *28*, 2333. (c) Haddon, R. C. *Aust. J. Chem.* **1975**, *28*, 2334.
(5) Peierls, R. C. *Quantum Theory of Solids*; Oxford University Press: London, 1953; p 108.
(6) Mott, N. F. *Metal−insulator Transitions*; Taylor and Frances: London, 1990.
(7) ΔH_{disp} is the enthalpy change for the conversion of two gas-phase radicals R into a cation/anion pair, i.e., $2\ R \rightleftarrows R^+ + R^-$, and accordingly is equal to the difference between the ionization potential (IP) and electron affinity (EA). The solution-based cell potential $E_{cell} = E_{1/2}(ox) - E_{1/2}(red)$ is the difference between the half-wave potentials for the oxidation and reduction processes.
(8) Kaszynski, P. *J. Phys. Chem. A* **2001**, *105*, 7626.
(9) Cordes, A. W.; Mingie, J. R.; Oakley, R. T.; Reed, R. W.; Zhang, H. *Can. J. Chem.* **2001**, *79*, 1352.
(10) Boeré, R. T.; Roemmele, T. L. *Coord. Chem. Rev.* **2000**, *210*, 369.

10.1021/ja0371350 CCC: $25.00

Chart 1

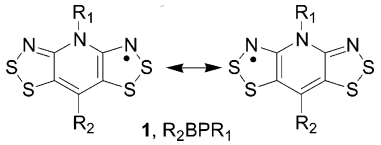

characterization of the first examples (R_2 = Cl, R_1 = Me, Et, and Pr) of this class of radical.[11] However, despite favorable ion energetics, the presence of the relatively bulky R_1/R_2 substituents led to slipped stack structures in which interannular overlap was severely reduced. The resulting loss of bandwidth *W* caused Mott insulating behavior.

In an attempt to modify the solid-state structural properties of these systems, and hence improve their conductivity, we have developed new and more flexible synthetic routes to the R_2-BPR_1 framework **1** (Chart 1). Herein we describe the preparation and structural characterization of the two prototypal radicals HBPMe and HBPEt **1** (R_2 = H; R_1 = Me, Et).[12] Variable-temperature magnetic susceptibility and single-crystal conductivity measurements have also been performed, and the results are discussed in the light of the extended Hückel band structure calculations.

Results

Synthesis. The first examples of the R_2BPR_1 framework were prepared by means of a double Herz condensation of 2,6-diaminopyridine with sulfur monochloride S_2Cl_2, which afforded the chloride salt of $[ClBPH]^+$ cation, i.e., [**1**][Cl] (R_2 = Cl, R_1 = H). Subsequent metathesis to a soluble hexafluorantimonate salt, and treatment of the latter with Proton Sponge liberated a zwitterionic base which, upon alkylation with alkyl triflates R_1-OTf (R_1 = Me, Et, Pr) and reduction of the so-formed triflate salts with decamethylferrocene, yielded $ClBPR_1$ radicals **1** (R_1 = Me, Et, Pr).[13] Though successful, this method was lengthy, especially the steps involving anion metathesis and salt purification.

We have now found that the double Herz methodology can be simplified by using 2,6-diaminopyridinium triflate **2** instead of 2,6-diaminopyridine as the starting material (Scheme 1). Under these conditions, a soluble triflate salt [**1**][OTf] (R_2 = Cl, R_1 = H) is produced in a single step, without the need for anion metathesis. Subsequent deprotonation of [**1**][OTf] (R_2 = Cl, R_1 = H) and realkylation of the resulting base provides an efficient route to [**1**][OTf] (R_2 = Cl; R_1 = Me, Et) derivatives. Alternatively, 2,6-diaminopyridine can be treated with an alkyl triflate R_1OTf to give **3**, and using this material a double Herz reaction leads directly to [**1**][OTf] (R_2 = Cl; R_1 = Me, Et) salts. This latter route is particularly appealing but is complicated by the fact that reaction of 2,6-diaminopyridine with alkyl triflates leads to alkylation of both the pyridine and exocyclic nitrogens.[14] When methyl triflate is used less than 20% of **3** (R_1 = Me) is obtained; other triflates give even poorer yields. This problem can be overcome by using the silylated diaminopyridine **4**. Alkylation of the latter with R_1OTf (R_1 = Me, Et) at the pyridine nitrogen is essentially quantitative, and deprotection of the subsequent salt **5** with $[Bu_4N][F]$ then affords the desired N-alkylated diaminopyridinium triflate **3**.

Scheme 1

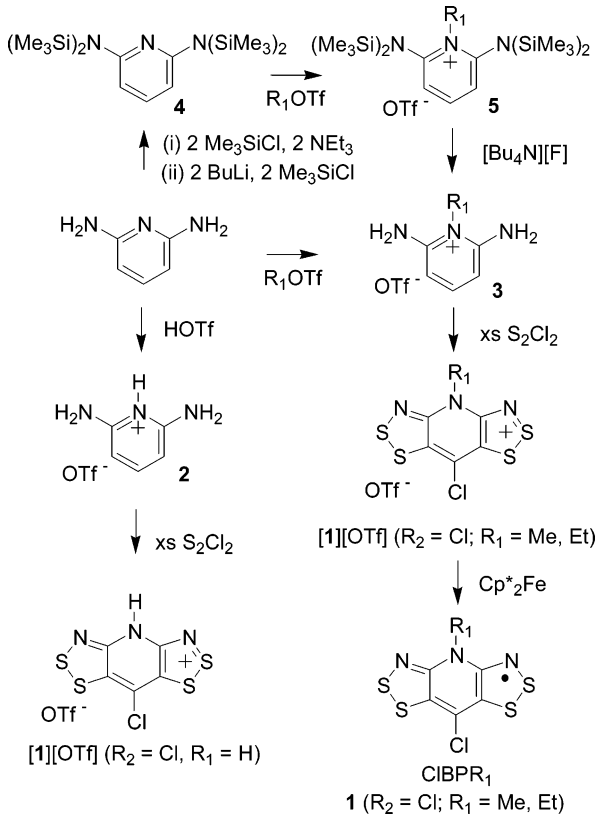

The double Herz cyclizations described above are all carried out at elevated temperatures, typically at reflux in CH_3CN, and these forcing conditions lead to chlorination of the 4-position of the pyridine ring. To prevent chlorination, and to open up routes to prototypal derivatives $HBPR_1$ (**1**, R_2 = H; R_1 = Me, Et), we explored several ambient temperature double Herz reactions. We found (Scheme 2) that the condensation of N-alkylated 2,6-diaminopyridinium triflates **3** with S_2Cl_2 in CH_3CN at room temperature in the presence of triethylamine as auxiliary base affords the desired chloride salts [**1**][Cl] (R_2 = H; R_1 = Me, Et) in good yield. Subsequent anion metathesis and reduction yields the prototypal radicals $HBPR_1$ (**1**, R_2 = H; R_1 = Me, Et). As an extension of this methodology, double-Herz cyclization of **4** with S_2Cl_2 in $C_2H_4Cl_2$ at room temperature provides the chloride salt [**1**][Cl] (R_2 = R_1 = H), which can be metathesized to the hexafluoroantimonate salt [**1**][SbF_6] (R_2 = R_1 = H) for characterization purposes.

EPR Spectra and Electrochemistry. The extent of spin delocalization in $HBPR_1$ radicals (R_1 = H, Me, Et) has been probed by EPR spectrometry and cyclic voltammetry. The X-band EPR spectra of $HBPR_1$ (R_1 = Me, Et), recorded in CH_2Cl_2 at room temperature, are similar to those observed for the corresponding $ClBPR_1$ (R_1 = Me, Et) radicals. The hyperfine pattern (Table 1) is dominated by coupling to two equivalent dithiazolyl nitrogens, the value of a_N being approximately one-

(11) Beer, L.; Brusso, J. L.; Cordes, A. W.; Haddon, R. C.; Itkis, M. E.; Kirschbaum, K.; MacGregor, D. S.; Oakley, R. T.; Pinkerton, A. A.; Reed, R. W. *J. Am. Chem. Soc.* **2002**, *124*, 9498.
(12) A preliminary account of the structural characterization of HBPMe has been published. See: Beer, L.; Brusso, J. L.; Cordes, A. W.; Haddon, R. C.; Godde, E.; Itkis, M. E.; Oakley, R. T.; Reed, R. W. *Chem. Commun.* **2002**, 2562.
(13) Beer, L.; Cordes, A. W.; Oakley, R. T.; Mingie, J. R.; Preuss, K. E.; Taylor, N. J. *J. Am. Chem. Soc.* **2000**, *122*, 7602.
(14) Similar problems have been encountered elsewhere. See, for example: Gilliot, P. *Bull. Soc. Chim. Fr.* **1934**, *1*, 796.

Scheme 2

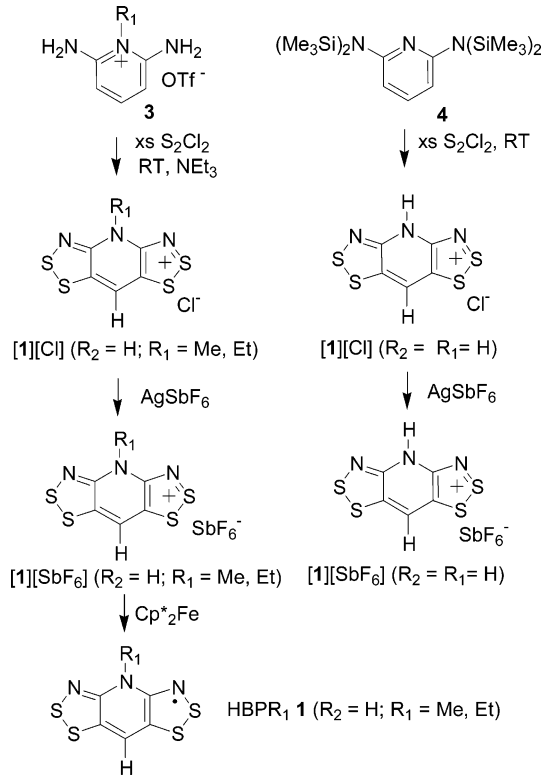

Table 1. EPR Hyperfine Coupling Constants (mT) and *g* Values for $HBPR_1$ **1**

compd		HBPH[a]	HBPMe	HBPEt
N(S)	a_N	0.357	0.313	0.318
$N(R_1)$	a_N	−0.069	0.062	0.061
H(C)	a_H	0.356	0.230	0.228
R_1(N)	a_H	−0.058 (NH)	0.034 (NCH_3)	<0.02 (NCH_2CH_3)
g value			2.0082	2.0082

[a] B3LYP/6-31G** values from a C_{2v} geometry optimization.

half of that observed in monofunctional 1,2,3-DTA radicals.[15] There is also weaker coupling to the pyridine nitrogen and to the *N*-methyl (or *N*-ethyl) protons. As an additional feature, the $HBPR_1$ (R_1 = Me, Et) radicals display hyperfine interactions with the CH proton of the pyridine residue. The experimental assignments have been cross-matched with the results of density functional theory calculations on a model HBPH radical, using the B3LYP method and a 6-31G** basis set.

The results of cyclic voltammetric measurements on the [**1**]-[SbF_6] salts (R_2 = H; R_1 = H, Me, Et) are summarized in Table 2. All members of the series show a reversible 0/+1 wave in the range −0.08 to −0.15 V vs SCE (Figure 1), individual values being shifted cathodically by some 120 mV with respect to analogous couples in the $ClBPR_1$ (**1**, R_2 = Cl; R_1 = H, Me, Et) compounds, as expected from the more electropositive core, and consistent with the calculated (B3LYP/6-31G**) IP and EA values of HBPH and ClBPH. A more anodic +1/+2 wave, also observed in the $ClBPR_1$ (R_1 = Me, Et) pair but at higher potentials, is also present. In contrast to the $ClBPR_1$ derivatives, where the −1/0 wave was fully reversible, the reduction wave

(15) (a) Cordes, A. W.; Mingie, J. R.; Oakley, R. T.; Reed, R. W.; Zhang, H. *Can. J. Chem.* **2001**, *79*, 1352. (b) Barclay, T. M.; Beer, L.; Cordes, A. W.; Oakley, R. T.; Preuss, K. E.; Taylor, N. J.; Reed, R. W. *Chem. Commun.* **1999**, 531. (c) Preston, K. F.; Sutcliffe, L. H. *Magn. Reson. Chem.* **1990**, *28*, 189.

Table 2. Solution Half-Wave[a] and Cell[b] Potentials (V) and Ion Energetics[c] for R_2BPR_1 **1**

	$E_{1/2}$(−1/0)	$E_{1/2}$(0/+1)	$E_{1/2}$(+1/+2)	E_{cell}	IP[c]	EA[c]	ΔH_{disp}[c]
ClBPH	*d*	0.035			6.30	1.60	4.70
ClBPMe	−0.835	0.005	1.415	0.84			
ClBPEt	−0.845	−0.018	1.390	0.83			
HBPH	*d*	−0.084			6.16	1.39	4.77
HBPMe	−0.95[e]	−0.130	1.294	0.77[f]			
HBPEt	−0.95[e]	−0.146	1.272	0.76[f]			

[a] In CH_3CN, ref SCE. [b] $E_{cell} = E_{1/2}(0/+1) - E_{1/2}(-1/0)$. [c] B3LYP/6-31G** values (in eV) from a C_{2v} geometry optimization (see the Experimental Section). [d] Irreversible behavior, see text. [e] Irreversible behavior, E_{pc} value quoted. [f] E_{cell} estimated as $E_{pc}(0/+1) - E_{pc}(-1/0)$.

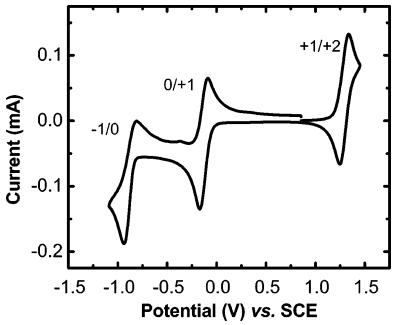

Figure 1. CV scan of [HBPMe][OTf] in CH_3CN, [*n*-Bu_4N][PF_6] supporting electrolyte.

for the $HBPR_1$ radicals is irreversible. This feature we also attribute to the more electropositive core of the radical, and a greater tendency toward cleavage of one of the S−S[16] (or S−N)[17] bonds upon reduction of the radical. The cell potential values E_{cell} cited in Table 2 are thus only estimates based on the difference between the cathodic peak potentials (E_{pc}) of the oxidation and reduction processes. Nonetheless the trends in both $E_{1/2}$ and E_{cell} map well onto those observed for $ClBPR_1$ radicals and are broadly consistent with the computed gas phase IP, EA, and disproportionation enthalpy (ΔH_{disp} = IP − EA) data. As seen before for ClBPH, the electrochemistry of HBPH is complicated by the proclivity of the NH proton to migrate with change in potential; as a result, only the 0/+1 wave is reversible for this system.[18] However, no EPR signal corresponding to the HBPH radical could be observed following chemical reduction of $[HBPH]^+$ salts.[19]

Crystal Structures. The crystal structures of $HBPR_1$ (R_1 = Me, Et) have been determined by X-ray crystallography. Crystals suitable for X-ray work were obtained by recrystallization from degassed dichloroethane; crystal data are summarized in Table 3. A summary of pertinent intra- and intermolecular distance and angle information is provided in Table 4. Figure 2 compares the unit cells of the two structures, as viewed down stacking axis, and Figure 3 illustrates the slipped π-stacks.

A comparison of the two structures reported here and those of the related $ClBPR_1$ (R_1 = Me, Et) compounds reported earlier reveals some interesting differences. Replacement of chlorine

(16) Antonello, S.; Benassi, R.; Gavioli, G.; Taddei, F.; Maran, F. *J. Am. Chem. Soc.* **2002**, *124*, 7529.
(17) Alternatively N−S bond cleavage could occur. See for example, Barclay, T. M.; Cordes, A. W.; Goddard, J. D.; Mawhinney, R. C.; Oakley, R. T.; Preuss, K. E.; Reed, R. W. *J. Am. Chem. Soc.* **1997**, *119*, 12136.
(18) Bechgaard, K.; Parker, V. D.; Pedersen, C. T. *J. Am. Chem. Soc.* **1973**, *95*, 4373.
(19) This parallels the behavior of [ClBPH][SbF_6] (see ref 11). In essence, we have been unable to isolate or even observe (by EPR) any R_2BPR_1 radical **1** with R_1 = H. Presumably reduction of the cation leads to migration of the NH proton, and rapid degradation of the consequent radical species.

Table 3. Crystallographic Data

compd	HBPMe	HBPEt
formula	$C_6H_4N_3S_4$	$C_7H_6N_3S_4$
fw	246.36	260.39
a, Å	3.9626(10)	4.9128(18)
b, Å	11.962(3)	14.764(5)
c, Å	18.262(5)	13.671(5)
β, deg	−	98.129(6)
V, Å^3	865.6(4)	981.6(6)
ρ(calcd), g cm^{-3}	1.890	1.762
space group	$P2_12_12_1$	$P2_1/c$
Z	4	4
T, K	293(2)	293(2)
μ, mm^{-1}	1.044	0.925
λ, Å	0.71073	0.71073
data/restraints/parameters	977/0/134	2246/0/151
solution method	direct methods	direct methods
R, *Rw* (on F^2)[a]	0.0338, 0.0597	0.0370, 0.0935

[a] $R = [\sum||F_o| - |F_c||]/[\sum|F_o|]$ for $I > 2\,\sigma(I)$; $R_w = \{[\sum w||F_o|^2 - |F_c|^2|^2]/[\sum(w|F_o|^4)]\}^{1/2}$.

Table 4. Summary of Intra- and Intermolecular Structural Parameters

compd		HBPMe	HBPEt
intramolecular distances (Å)[a]			
	S−S	2.097(10)	2.101(12)
	S−N	1.660(3)	1.660(10)
intermolecular contacts[b] (Å) and angles (deg)			
d1	S1−S3′	3.371(1)	3.353(1)
d2	S2−S3′	3.666(1)	3.744(1)
d3	S2−S3″	3.745(1)	3.622(1)
τ[c]		62.04(7)	47.1(1)
δ[c]		3.500(6)	3.598(8)

[a] Bond lengths cited are average values; numbers in parentheses are the larger of the ESD or the range. [b] See Figure 3 for definitions of d1−d3. [c] See Figure 4 for definitions of τ and δ.

by hydrogen does not alter the space group ($P2_12_12_1$) for the R_2BPMe (R_2 = Cl, H) pair, and in both structures the radicals form slipped π-stacks clustered about 2_1 axes. By contrast the R_2BPEt (R_2 = Cl, H) pair are not isomorphous, adopting the space groups, $P\bar{4}2_1m$ and $P2_1/c$, respectively. In the former, the radical π-stacks cluster about $\bar{4}$ centers, while in the latter they spiral about 2_1 axes. The arrangement of the slipped stacks is also very different in the two compounds. By contrast, comparison of the HBPR_1 pair (R_1 = Me, Et) reveals that while the space groups are different, the crystal packing is quite similar. In both cases the radicals form ribbonlike arrays (Figure 2), along *z* in HBPMe and *y* in HBPEt, with molecules clustering about 2_1 axes and $\bar{1}$ points, respectively. The radicals form slipped π-stacks along the *x*-direction that lock together into a tightly knit herringbone pattern (Figure 3). Between the stacks there is one intermolecular S- - -S contact (d1 = S1- - -S3′) significantly shorter than the van der Waals separation (3.6 Å) for two sulfurs,[20] as well as others (d2, d3) in the range 3.6−3.7 Å (Table 4).

It is readily apparent from Figure 3 that the π-stacks are more steeply inclined in HBPEt than in HBPMe. The degree of inclination in R_2BPR_1 derivatives can be quantified in terms of the tilt or slippage angle τ, defined as the angle between the mean molecular plane of the radical and the stacking axis—a smaller value of τ indicates a higher degree of slippage (Figure 4). Thus, the value of τ for HBPMe (62.04(7)°) is greater than

(20) Bondi, A. *J. Phys. Chem.* **1964**, *68*, 41.

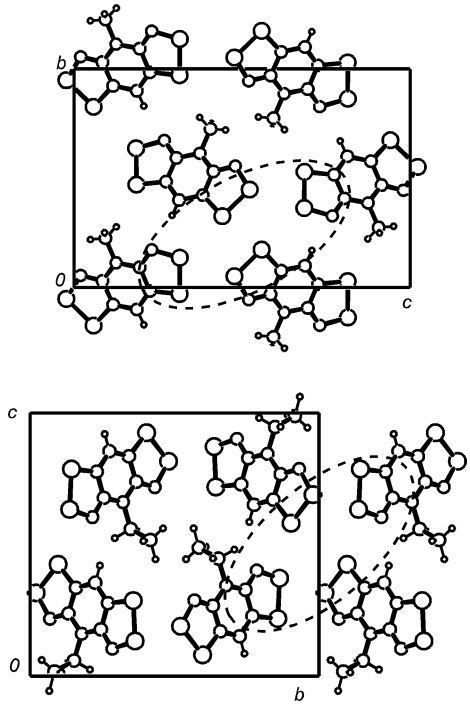

Figure 2. Unit cells of HBPMe (above) and HBPEt (below). Clustering of radicals about 2_1 axes (above) and inversion centers (below) are shown with hatched ovals.

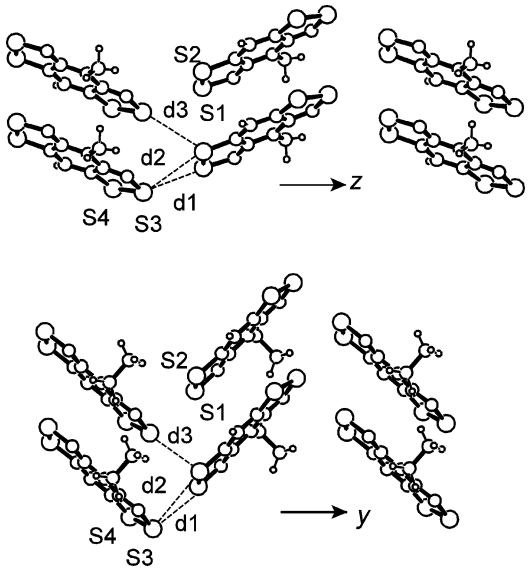

Figure 3. Herringbone packing of radical π-stacks in HBPMe (above) and HBPEt (below). Intermolecular S- - -S contacts are defined in Table 4.

that in ClBPMe (54.81(13)°) at 293 K; i.e., the molecular planes are more nearly superimposed in the former, a trend which might be expected from the replacement of the sterically bulky chlorine by a hydrogen atom. At the same time, however, the plane-to-plane separation δ increases, from 3.470(5) Å in ClBPMe to 3.500(6) Å in HBPMe, suggesting that radicals separate slightly to alleviate repulsive Me- - -Me interactions. In HBPEt, the value of τ (47.1(1)°) is the smallest to date for any R_2BPR_1 structure, while the value of δ (3.598(8) Å) is the largest. Such a combination might be construed as leading to a reduction in intrastack overlap but, as the band calculations below indicate, this is not the case.

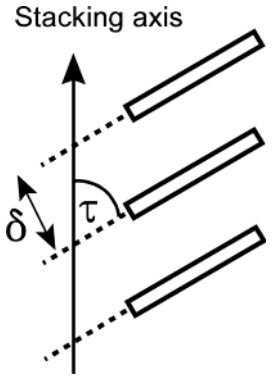

Figure 4. Definition of slippage angle τ and plane-to-plane separation δ.

Table 5. Magnetic Susceptibility[a] and Conductivity Data

compd	HBPMe	HBPEt
χ_0, emu mol^{-1}	-120.4×10^{-6}	-132.2×10^{-6}
C, emu mol^{-1}	0.345[b]	0.343[c]
Θ, K	0[b]	−4.5[c]
σ(300 K), S cm^{-1}	2.3×10^{-6}	7.5×10^{-6}
E_a,[d] eV	0.41	0.41

[a] C and Θ obtained from Curie−Weiss fits, i.e., $\chi = C/(T - \Theta)$. [b] From the data above 85 K. [c] From the data above 4.5 K. [d] E_a corresponds to the activation energy of the conductivity; for an intrinsic semiconductor and temperature independent mobility the optical band gap $E_g = 2E_a$.

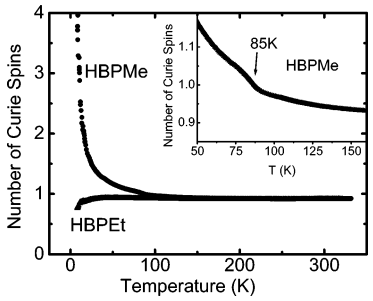

Figure 5. Curie Spin count of $HBPR_1$ (R_1 = Me, Et) as a function of temperature. The inset shows an expansion of the 50−150 K region for HBPMe.

The intramolecular parameters for the radical rings in HBPMe and HBPEt are all nominal, the mean S−S and S−N distances lying close to those seen in the ClBPR series, and longer than those in oxidized rings, as expected from the antibonding nature of the radical SOMO.

Magnetic and Conductivity Measurements. Variable-temperature magnetic susceptibility (χ) measurements have been carried out on microcrystalline samples of $HBPR_1$ (R_1 = Me, Et). The temperature dependences of χ for both compounds show normal Curie−Weiss[21] behavior for $S = {}^1/_2$ systems between 330 and 100 K; values of χ_0, C, and Θ are provided in Table 5, and a plot of the effective number of Curie spins N relative to that expected for a $S = {}^1/_2$ system ($N = \chi T/0.375$) is provided in Figure 5. HBPEt shows a decrease in the number of Curie spins with decreasing temperature below 50 K, which corresponds to a weakly antiferromagnetic coupling. In contrast, HBPMe demonstrates an increase in the number of Curie spins with decreasing temperature below 100 K accompanied by a small steplike change in N value at 85 K (see inset in Figure 5). This behavior, an apparent phase change to a weakly ferromagnetically coupled state, was also observed in ClBPMe (at 93 K), but the transition was more pronounced and accompanied by a hysteretic temperature dependence of χ.[11]

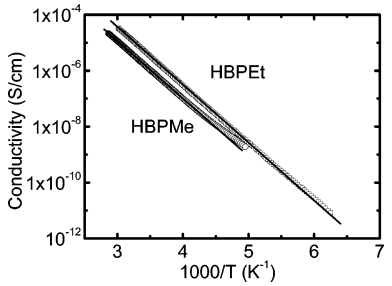

Figure 6. Log plots ofσ vs $1/T$ for $HBPR_1$ (R_1 = Me, Et).

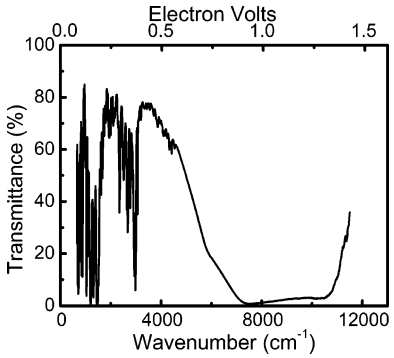

Figure 7. Single-crystal IR and near-IR transmission spectrum of crystalline HBPEt.

Below 14 K an antiferromagnetic "tail" is evident. This latter feature is not observed in HBPMe; indeed, for this system the Curie spin count continues to increase past its value of 7.3 at 5 K, the limit of the measurement.

Electrical conductivity (σ) measurements along the needle axes of $HBPR_1$ (R_1 = Me, Et) have been performed over the temperature range 150−330 K; Figure 6 shows log plots of σ against $1/T$ for the two compounds. As can be seen, the conductivity is activated, with values of σ at 300 K increasing from near 10^{-6} S cm^{-1} for R_1 = Me to near 10^{-5} S cm^{-1} for R_1 = Et (Table 5). The derived thermal activation energies E_a are essentially identical at 0.41 eV.

Near-Infrared Spectrum of HBPEt. To extract information on the excited-state electronic structure of R_2BPR_1 radicals in general, and HBPEt in particular, we have measured the near-infrared spectrum of a crystalline sample of HBPEt. The results are presented in Figure 7, which shows the transmittance over the range 650−11000 cm^{-1}. The absorptions in the mid-IR region between 650 and 3100 cm^{-1} are due to molecular vibrations of the radical. As may be seen, there is a well-developed, low-lying absorption band with a bandwidth of about 1 eV. The optical energy gap E_g has a threshold value of 0.45 eV increasing to near 0.9 eV at the mobility edge.

Band Structures. To place the magnetic, conductivity, and optical properties in context, we have probed the solid-state band structures of the pair of $HBPR_1$ (R_1 = Me, Et) radicals by extended Hückel theory (EHT) methods. The results must be viewed with caution, as the approach cannot be expected to succeed in systems where the tight-binding approximation fails, i.e., in Mott insulators. Figure 8 shows EHT dispersion curves, plotted along the stacking direction,[22] of the four crystal orbitals

(21) Carlin, R. L. *Magnetochemistry*; Springer-Verlag: New York, 1986.
(22) HBPMe is a tetragonal structure, and there is an exact equivalence of the directions of the unit cell vectors in real and reciprocal space. HBPEt is monoclinic, and the correspondence between real and reciprocal space directions is only approximate.

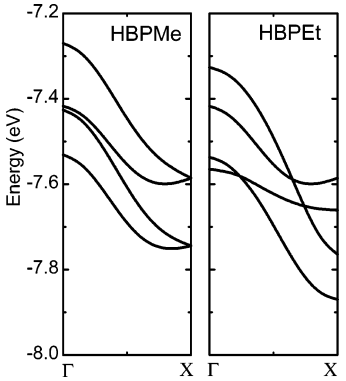

Figure 8. EHT dispersion curves for $HBPR_1$ (R_1 = Me, Et) radicals.

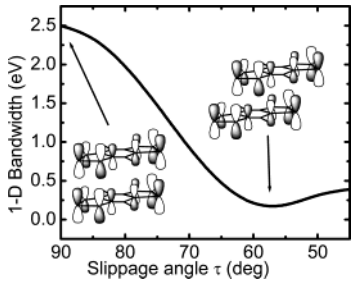

Figure 9. EHT bandwidth W of a model 1-D stack of HBPH radicals as a function of lateral slippage angle τ. The intermolecular spacing, δ, is set at 3.45 Å.

(COs) arising from the SOMOs of the four radicals in the unit cell. These curves would constitute the half-filled conduction band if the materials were molecular metals. To this extent the calculations clearly fail to describe the ground-state electronic structure. The magnetic measurements confirm that, at ambient temperature, all the electrons are unpaired (the materials are not Pauli paramagnets), and the conductivity is activated (not metallic). But the dispersion curves nonetheless provide insight into the extent of the intermolecular interactions along and perpendicular to the slipped π-stacks. The total bandwidth W ranges from 0.4 to 0.5 eV (similar to those found for the $ClBPR_1$ compounds) and is comprised of contributions from orbital interactions transverse to as well as along the stacking axis, although clearly the latter dominates.

While these estimates of W are in keeping with bandwidths found in conventional organic conductors, the values were smaller than we had expected. To explore the structural causes for the reduced bandwidth we carried out a series of EHT calculations on model structures consisting of a 1-D stack of HBPH radicals set at a plane-to-plane separation (δ) of 3.45 Å. The bandwidth W for the $^1/_2$-filled energy band arising from orbital interactions between the π-SOMOs was calculated, within the EHT framework, over a series of slippage angles τ, ranging from $\tau = 90°$ to $\tau = 45°$. The results, plotted in Figure 9, reveal that superimposed ($\tau = 90°$) R_2BPR_1 π-stacks are associated with extremely large bandwidths W, in excess of 2 eV for δ values less than 3.5 Å. However, as slippage of the radicals takes place, a displacement necessitated at least in part by steric interactions between the exocyclic R-groups, the magnitude of W drops dramatically. The change can be rationalized in terms of the nodal properties of the antibonding SOMO of R_2BPR_1 radicals. As lateral plate slippage takes place, overlap drops off rapidly, reaching a minimum around $\tau = 55-60°$, i.e., the experimentally observed region. The loss of

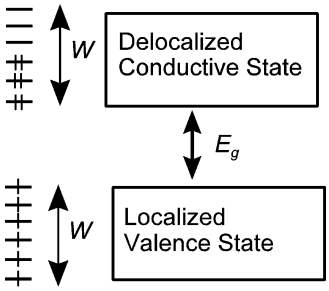

Figure 10. Electronic structure of solid R_2BPR_1 radicals.

bandwidth arising from the near orthogonality of intermolecular overlap can be related to the onset of ferromagnetic coupling observed in HBPMe (and ClBPMe).[23,24] Interestingly, slippage beyond values of τ less than 55° leads to a slight increase in bandwidth, and we believe that this feature is the root cause for the greater dispersion observed in HBPEt.

Discussion

The EHT band calculations on the crystal structures of $HBPR_1$ (R_1 = Me, Et) suggest a reasonably well-developed band structure, but without the inclusion of electron correlation the method clearly fails to provide an accurate description of the ground-state electronic structure of the radicals. If the materials were metallic, the bands shown in Figure 8 would be half-filled, but the magnetic and conductivity measurements suggest otherwise. The materials are Curie paramagnets above 100 K, rather than Pauli paramagnets, and the conductivity is activated.

These features point to a Mott−Hubbard insulator with a localized valence state in which each of the levels in the band, of bandwidth W, is half-filled (Figure 10).[25] In the present systems the localized spins show weak magnetic interactions along the π-stack, ferromagnetic for HBPMe and antiferromagnetic for HBPEt. The delocalized conductive state is separated from the insulating state by an energy gap E_g. From the optical measurements the value of E_g can be estimated at 0.45 eV using the threshold excitation energy, or near 0.9 eV at the mobility edge. Assuming intrinsic semiconductor behavior (for which $E_a = {}^1/_2E_g$), the latter (mobility edge) value matches quite well with the thermal activation energies E_a derived from the conductivity measurements (Table 5). By using the Mott−Hubbard condition $U \sim W + E_g$, and the bandwidths obtained from the EHT calculations, the onsite Coulomb repulsion U for these radicals can be estimated to be near 1.0 eV.

Given this picture of the electronic structure of the radicals, and assuming that only the thermally activated electrons contribute to the conductivity, we can estimate the mobility (μ) of the carriers from the relationship $\sigma = ne\mu$, where σ is the conductivity and e the charge on an electron. Accordingly, we find $\mu = 0.02$ cm^2/Vs for HBPMe and 0.09 cm^2/Vs for HBPEt, typical values for organic superconductors.[26]

(23) Takano, Y.; Taniguchi, T.; Isobe, H.; Kubo, T.; Morita, Y.; Yamamoto, K.; Nakasuji, K.; Takui, T.; Yamaguchi, K. *J. Am. Chem. Soc.* **2002**, *124*, 11122.
(24) (a) Verdaguer, M. *Polyhedron* **2001**, *20*, 1115. (b) Hicks, R. G.; Lemaire, M. T.; Richardson, J. R.; Thompson, L. K.; Xu, Z. *J. Am. Chem. Soc.* **2001**, *123*, 7154. (c) Manson, J. L.; Arrif, A. M.; Miller, J. S. *Chem. Commun.* **1999**, 1479.
(25) (a) Whangbo, M.-H. *J. Chem. Phys.* **1979**, *70*, 4963. (b) Landrum, G. A.; Dronkowski, R. *Angew. Chem., Int. Ed.* **2000**, *39*, 1560.
(26) Murata, K.; Ishibashi, M.; Honda, Y.; Fortune, N. A.; Tokumoto, M.; Kinoshita, N.; Anzai, H. *Solid State Commun.* **1990**, *76*, 377.

Conclusion and Summary

The development of molecular conductors based on neutral radical building blocks faces a series of design challenges. The key structural problem is a Peierls instability—the tendency of radicals to dimerize—which we have sought to overcome by using heterocyclic radicals, in which C−C dimerization can generally be suppressed (although other modes of association, e.g., through S- - -S bonds, are possible). The major electronic problem is the large on-site Coulomb repulsion energy U, overcoming which requires the development of much softer[27] radicals with gas-phase disproportionation energies even less than those found for metallic elements, where electronic bandwidths are much larger.

Highly delocalized dithiazolodithiazolyl radicals R_2BPR_1 address both of these issues directly. Their calculated gas-phase disproportionation enthalpies and measured electrochemical cell potentials are superior to those of all previously known heterocyclic radicals, and the presence of the "beltline" R_1 and R_2 groups precludes the possiblity of cofacial dimerization. At the same time, however, slippage of the radical π-stacks leads to a loss of intermolecular overlap, and a localized Mott−Hubbard insulator ground state. In the case of HBPMe (and ClBPMe) this loss of bandwidth is associated with weak ferromagnetic coupling along the π-stack.

The synthetic advances described herein, involving a "double Herz" reaction on a protonated or N-alkylated 2,6-diaminopyridinium salt, provide a simple *one-step* method for the construction of $ClBPR_1$ and $HBPR_1$ derivatives, thereby paving the way for the development of a wide range of R_2BPR_1 derivatives. Changes in molecular structure will allow modifications in crystal packing and, hopefully, materials with increased bandwidth W. This being the case, single-component neutral radical materials with improved and even metallic conductivity may be accessible.

Experimental Section

General Procedures and Starting Materials. The reagents 2,6-diaminopyridine, chlorotrimethylsilane, *n*-butyllithium (1.6 M in hexane), sulfur monochloride, gallium trichloride, silver hexafluoroantimonate, methyl and ethyl trifluoromethansulfonates (triflates), trifluoromethanesulfonic acid (triflic acid), Proton Sponge, triethylamine, and decamethylferrocene were obtained commercially (all from Aldrich) and used as received. All solvents were of at least reagent grade; acetonitrile and dichloroethane were dried by distillation from P_2O_5; diethyl ether was dried by distillation from $LiAlH_4$. All reactions were performed under an atmosphere of dry nitrogen. Melting points are uncorrected. Infrared spectra (Nujol mulls, KBr optics) were recorded on a Nicolet Avatar FTIR spectrometer (at 2 cm^{-1} resolution) and visible spectra were collected using a Beckman DU 640 Spectrophotometer. ^1H NMR spectra were run on a Bruker Avance 300 MHz NMR spectrometer. Low-resolution mass spectra (70 eV, EI/DEI and CI/DCI) were run on a Finnigan 4500 quadrupole mass spectrometer at the McMaster Regional Centre for Mass Spectrometry. Elemental analyses were performed by MHW Laboratories, Phoenix, AZ.

Preparation of 2,6-Diaminopyridinium Triflate 2. Triflic acid (6.90 g, 63.2 mmol) was added dropwise to a solution of 2,6-diaminopyridine (9.00 g, 66.6 mmol) in 300 mL of dichloroethane at 40 °C. A heavy white precipitate formed almost immediately. Once the addition was complete, the reaction was removed from heat and stirred for 2 h at room temperature and then left to stand in an ice bath for 1 h. The product, 2,6-diaminopyridinium triflate **2**, was filtered off, washed with dichloroethane, and dried in vacuo; yield 14.2 g, 54.8 mmol, 87%. Recrystallization from dichloroethane/acetonitrile (9:1) afforded colorless plates, mp 120−21 °C. ^1H NMR (δ, CD_3CN): 11.02 (s, br, 1NH), 7.51 (t, 1H, J = 8.4 Hz), 6.01 (d, 2H, J = 8.4 Hz), 4.46 (s, 2H, NH). IR: 3420 (s), 3350 (s), 3235 (s), 3153 (s), 3017 (s), 1662 (vs), 1492 (w), 1308 (s), 1260 (vs), 1180 (s), 1167 (s), 1032 (s), 994 (w), 795 (m), 763 (vw), 719 (w), 641 (m), 580 (m), 566 (w), 517 (m), 477 (w), 429 (w) cm^{-1}. Anal. Calcd for $C_6H_3N_3F_3O_3S$: C, 27.80; H, 3.11; N, 16.21. Found: C, 28.00; H, 2.91; N, 16.22.

Preparation of 8-Chloro-4*H*-bis[1,2,3]dithiazolo[4,5-b:5′,4′-e]pyridin-2-ium Triflate [1][OTf] (R_2 = Cl, R_1 = H). Sulfur monochloride (20 mL, 33.7 g, 250 mmol) was added to a stirred solution of 2,6-diaminopyridinium triflate **2** (6.60 g, 25.0 mmol) in 150 mL of CH_3CN, and the resulting mixture was heated to reflux to produce a dark green solution. After 16 h, the reaction mixture was cooled to room temperature and the crude [**1**][OTf] (R_2 = Cl, R_1 = H), a dark red solid, filtered off, washed with 150 mL of CH_3CN followed by 2 × 150 mL of dichloroethane, and dried in vacuo. The crude product (6.73 g, 16.2 mmol, 64%) was boiled in 400 mL of dichloroethane to remove traces of sulfur and then recrystallized from 650 mL of acetonitrile (the solution concentrated to 400 mL after hot filtration) to afford red crystalline plates of [**1**][OTf] (R_2 = Cl, R_1 = H), yield 3.36 g (8.07 mmol, 50% from crude), dec > 250 °C. ^1H NMR (δ, CD_3CN): 2.20 (s, 1H, NH). IR: 1553 (w), 1510 (vw), 1338 (s), 1275 (w), 1245 (s), 1183 (s), 1125 (w), 1110 (m), 1026 (s), 850 (m), 841 (m), 766 (s), 715 (vw), 675 (w), 632 (s), 575 (w), 522 (m), 511 (m), 488 (vw), 469 (m) cm^{-1}. Anal. Calcd for $C_6HN_3F_3O_3ClS_5$: C, 17.33; H, 0.24; N, 10.10. Found: C, 17.25; H, 0.10; N, 9.87.

Preparation of 2,6-*N*,*N*,*N*′*N*′-Tetrakis(trimethylsilyl)diaminopyridine 4. A mechanically stirred mixture of triethylamine (153.0 mL, 1.1 mol), diaminopyridine (54.5 g, 0.50 mol), and chlorotrimethylsilane (140.0 mL, 1.10 mol) in 1.0 L of toluene was heated at 80 °C for 48 h. A white precipitate of triethylamine hydrochloride was filtered off, and the solvent flash distilled from the filtrate to leave a light brown oil. Vacuum distillation at 120 °C/10^{-1} Torr afforded 2,6-*N*,*N*′-bis-(trimethylsilyl)diaminopyridine as a colorless oil, yield 108.1 g (0.43 mol, 85.4%). IR: 3394 (m), 2955 (m), 2899 (m), 1596 (vs), 1581 (vs), 1456 (vs), 1394 (s), 1357 (m), 1342 (w), 1301 (s), 1283 (s), 1252 (s), 1150 (m), 1092 (w), 1041 (m), 1029 (m), 893 (s), 842 (s), 783 (s), 737 (m), 721 (m), 692 (m), 667 (w), 623 (w), 501 (w), 444 (m), 414 (w) cm^{-1}. ^1H NMR (δ, $CDCl_3$): 7.08 (t, 1H, J = 7.9 Hz), 5.78 (d, 2H, J = 7.9 Hz), 4.46 (s, 2H, NH), 0.23 (s, 18H, Si*Me*$_3$). Without further purification, this material (82.7 g, 0.33 mol) was dissolved in 800 mL of diethyl ether and treated with *n*-BuLi (400 mL, 1.6 M, 0.64 mol) and the solution stirred for 4 h. Chlorotrimethylsilane (81.0 mL, 0.64 mmol) was added and the mixture stirred for 16 h. The solution was filtered (by cannula) from the white precipitate of LiCl and the solvent flash distilled to leave a tan-colored oil. Vacuum distillation afforderd a colorless oil, bp 120 °C/10^{-1} Torr, which solidified on standing to a white solid **4**, yield 100.4 g (0.25 mol, 77.2%). The compound was recrystallized from a 1:1 mixture of acetonitrile/toluene as colorless needles, mp 43−45 °C. IR: 1577 (vs), 1561 (vs), 1295 (s), 1250 (vs), 1228 (vs), 1152 (w), 1088 (w), 1038 (vs), 989 (m), 948 (vs), 905 (vs), 847 (vs), 792 (m), 758 (s), 741 (s), 681 (s), 653 (w), 622 (m), 523 (w), 460 (w) cm^{-1}. ^1H NMR (δ, $CDCl_3$): 7.34 (t, 1H, J = 7.7 Hz), 6.44 (d, 2H, J = 7.7 Hz), 0.13 (s, 36 H, *Me*$_3$Si). Anal. Calcd for $C_{17}H_{39}N_3Si_4$: C, 51.32; H, 9.88; N, 10.56. Found: C, 51.43; H, 9.80; N, 10.80.

Preparation of *N*-Methyl-2,6-*N*,*N*,*N*′*N*′-tetrakis(trimethylsilyl)-diaminopyridinium Triflate 5 (R_1 = Me). A solution of methyl triflate (20.0 g, 0.122 mol) in 50 mL was added to a stirred solution of **4** (40.0 g, 0.101 mol) in 500 mL diethyl ether at 0 °C to afford a heavy white precipitate. After 4 h, the analytically pure *N*-methyl triflate **5** was filtered off and washed with 2 × 50 mL diethyl ether. The filtrate was cooled at −20 °C overnight to precipitate more product, which was collected by filtration and washed with a minimum amount of

(27) (a) Pearson, R. G. *Struct. Bonding (Berlin)* **1993**, *80*, 2. (b) Pearson, R. G. *J. Chem Educ*. **1988**, *64*, 561.

diethyl ether. The combined solids were dried in vacuo, yield 52.5 g (0.094 mol, 93%), dec > 220 °C. IR: 3436 (m), 3359 (s), 3243 (s), 1665 (s), 1640 (s), 1584 (s), 1516 (s), 1334 (w), 1299 (m), 1263 (s), 1227 (s), 1162 (s), 1030 (s), 786 (m), 758 (w), 640 (s), 576 (m), 519 (m) cm^{-1}. ^1H NMR (δ, $CDCl_3$): 8.52 (t, 1H, $J = 9.2$ Hz), 7.33 (d, 2H, $J = 9.2$ Hz), 3.97 (s, 3H, CH_3), 0.20 (s, 36 H, Me_3Si). Anal. Calcd for $C_{19}H_{42}F_3N_3O_3SSi_4$: C, 40.61; H, 7.53; N, 7.48. Found: C, 40.73; H, 7.32; N, 7.60.

Preparation of *N*-Ethyl-2,6-*N*,*N*,*N*′*N*′-tetrakis(trimethylsilyl)-diaminopyridinium Triflate 5 (R_1 = Et). Neat ethyl triflate (4.0 mL, 0.031 mol) was added to solid **4** (10.0 g, 0.025 mol) and the mixture heated in an oil bath at 60 °C. After 10 min, the molten mixture solidified to a white crystalline solid. This was dissolved in 5 mL of CH_3CN then reprecipitated by addition of diethyl ether. The product **5** (R_1 = Et) was collected by filtration, washed with diethyl ether, and dried in vacuo, yield 12.4 g (0.022 mol, 85%), dec > 180 °C. IR: 1605 (m), 1556 (m), 1267 (vs), 1223 (m), 1176 (w), 1152 (vs), 1107 (m), 1081 (w), 1031 (s), 990 (s), 917 (vs), 897 (s), 850 (vs), 827 (s), 763 (m), 747 (m), 690 (w), 670 (w), 637 (s), 627 (w), 572 (w), 517 (w), 458 (w) cm^{-1}. ^1H NMR (δ, $CDCl_3$): 8.14 (t, 2H, $J = 8.0$ Hz), 7.29 (d, 1H, $J = 8.0$ Hz), 4.55 (q, 2H, CH_2CH3, $J = 7.2$ Hz), 1.49 (t, 3H, CH_2CH_3, $J = 7.2$ Hz), 0.22 (s, 36 H, Me_3Si). Anal. Calcd for $C_{20}H_{44}F_3N_3O_3SSi_4$: C, 41.70; H,7.70; N, 7.30. Found: C, 41.80; H, 7.96; N, 7.48.

Preparation of *N*-Methyl-2,6-diaminopyridinium Triflate 3 (R_1 = Me). Route 1. A solution of methyl triflate (50.0 g, 0.305 mol) in 50 mL of dichloroethane was added dropwise to a slurry of 2,6-diaminopyridine (36.4 g, 0.334 mol) in 500 mL of dichloroethane at 0 °C and the mixture stirred for 1 h. A white crystalline solid (a mixture of protonated and *N*-methylated diaminopyridinium salts **2** and **3**) was collected by filtration, washed with 50 mL of dichloroethane, and dried in vacuo. The protonated material was removed by stirring the crude mixture in a solution of 20 mL of triethylamine in 250 mL of dichloroethane for 1 h. The remaining solid was collected by filtration, washed with 50 mL of diethyl ether, and dried in vacuo, yield 13.8 g (0.051 mol, 16%). The product **3** was recrystallized from 450 mL of a hot solution of acetonitrile/dichloroethane (1:9 by volume), yield 10.3 g (0.038 mol, 75%), mp = 169−71 °C. IR: 3436 (m), 3358 (s), 3241 (s), 1665 (s), 1640 (s), 1584 (s), 1515 (s), 1300 (s), 1263 (vs), 1226 (vs), 1161 (vs), 1029 (vs), 786 (m), 758 (m), 640 (s), 575 (m), 518 (s), 452 (w) cm^{-1}. ^1H NMR (δ, CD_3CN): 7.49 (t, 2H, $J = 8.3$ Hz), 6.18 (d, 3H, $J = 8.3$ Hz), 6.04 (s, amino), 3.43 (s, methyl). Anal. Calcd. for $C_7H_{10}F_3N_3O_3S$: C, 30.77; H, 3.69; N, 15.38. Found: C, 30.92; H, 3.75; N, 15.50. **Route 2.** A solution of tetra-*n*-butylammonium fluoride (5 mL, 0.1 M solution) and methanol (20 mL, 0.493 mol) in THF was added to a solution of **5** (R_1 = Me, 52.5 g, 0.094 mol) in 500 mL of dichloroethane at 0 °C. Within minutes, a heavy white precipitate formed. The mixture was stirred for 4 h and the solution warmed to just below reflux; acetonitrile was added slowly until all solids dissolved. The solution was cooled to 0 °C and the crystalline product **3** (R_1 = Me) collected by filtration. A second crop was obtained by concentrating the filtrate almost to dryness, followed by the addition of more dichloroethane. This was collected by filtration and washed with dichloroethane. The combined crops were dried in vacuo, yield 25.1 g (0.091 mol, 97%). Spectroscopic data were identical to those for material prepared via route 1.

Preparation of *N*-Ethyl-2,6-diaminopyridinium Triflate 3 (R_1 = Et). Tetrabutylammonium fluoride in THF (0.40 mL, 0.40 mmol) was added to a stirred solution of **5** (R_1 = Et, 12.0 g, 0.021 mol) and methanol (2.7 g, 0.084 mol) in 50 mL of dichloroethane. After 1 h, a heavy white precipitate began to form. The reaction mixture was cooled to −20 °C for an additional 1 h and the precipitate collected by filtration, washed with diethyl ether, and dried in vacuo. The product **3** (R_1 = Et) was recrystallized from a mixture of hot dichloroethane (120 mL) and acetonitrile (15 mL), yield 5.93 g (0.021 mol, 99%), mp 98−99 °C. IR: 3424 (s), 3358 (s), 3289 (m), 3247 (s), 3091 (w), 1676 (s), 1652 (s), 1583 (s), 1513 (s), 1411 (w), 1338 (m), 1263 (vs), 1168 (s), 1068 (m), 1032 (vs), 963 (w), 786 (s), 761 (w), 737 (w), 709 (w), 639 (s), 573 (w), 513 (m) cm^{-1}. ^1H NMR (δ, CD_3CN): 7.46 (t, 1H, $J = 8.3$ Hz), 6.16 (d, 2H, $J = 8.3$ Hz), 6.10 (s, 4H, NH_2), 3.93 (q, 2H, CH_2CH_3, $J = 7.4$ Hz), 1.33 (t, 3H, CH_2CH_3, $J = 7.4$ Hz). Anal. Calcd for $C_8H_{12}F_3N_3O_3S$: C, 33.45; H, 4.21; N, 14.63. Found: C, 33.53; H, 4.34; N, 14.80.

Preparation of 8-Chloro-4-methyl-4*H*-bis[1,2,3]dithiazolo[4,5-*b*:5′,4′-*e*]pyridin-2-ium Trifluoromethanesulfonate [1][OTf] (R_2 = Cl, R_1 = Me). Sulfur monochloride (15 mL, 25.3 g, 187 mmol) was added to a solution of **3** (R_1 = Me, 4.93 g, 18.0 mmol) in 100 mL of acetonitrile and the resulting mixture heated to reflux to produce a dark green solution. After 16 h, the reaction mixture was cooled to room temperature to afford [ClBPMe][OTf], [**1**][OTf] (R_2 = Cl, R_1 = Me), as a dark red solid. The crude product was collected by filtration, washed with 100 mL of acetonitrile followed by 2 × 100 mL of dichloethane and dried in vacuo, yield 6.07 g (14.1 mmol, 78%). The crude product was extracted with hot dichloroethane to remove traces of sulfur and then recrystallized from 700 mL of acetic acid to afford deep red crystalline plates, the IR spectrum of which was identical to that of a sample obtained by an alternate route.[11] ^1H NMR (δ, CD_3CN): 3.57 (s, 3H, NMe).

Preparation of 4-Methyl-4*H*-bis[1,2,3]dithiazolo[4,5-*b*:5′,4′-*e*]pyridin-2-ium Hexafluoroantimonate [1][SbF_6] (R_2 = H, R_1 = Me). A solution of triethylamine (31.5 mL, 0.226 mol) in 30 mL of acetonitrile was added dropwise to a stirred solution of sulfur monochloride (7.7 mL, 0.095 mol) and **3** (R_1 = Me, 10.3 g, 0.0377 mol) in 200 mL of acetonitrile at 0 °C. Once the addition was complete, the flask was sealed and stirred for 5 days. The resulting blue/black precipitate, crude [HBPMe][Cl], [**1**][Cl] (R_2 = H, R_1 = Me), was collected by filtration, washed with 100 mL of acetonitrile, followed by 100 mL of dichloroethane, and dried in vacuo, yield 17.6 g. Solid gallium trichloride (14.2 g, 0.081 mol) was added to a slurry of the crude product (17.6 g, 0.0627 mol) in 100 mL of acetonitrile, and the deep green/blue solution so formed stirred for 30 min. A small amount of black insoluble material was filtered off and the solvent removed from the filtrate by flash distillation. The deep red solid residue, [HBPMe][$GaCl_4$], [**1**][$GaCl_4$] (R_2 = H, R_1 = Me), so obtained was washed with 3 × 100 mL of acetic acid, collected by filtration, and dried in vacuo, yield 8.2 g (0.018 mol, 29%). The product was dissolved in 120 mL of acetonitrile and 10 mL of pyridine added to afford a dark purple precipitate of purified [HBPMe][Cl]. This purified powder was collected by filtration, washed with 2 × 50 mL of acetonitrile, and dried in vacuo, yield 4.2 g (0.015 mol, 83% from [HBPMe][$GaCl_4$]), dec > 250 °C. IR: 1510 (w), 1377 (m), 1292 (m), 1148 (vw), 1022 (m), 949 (vw), 876 (vw), 850 (w), 737 (m), 716 (m), 654 (m), 530 (vw), 500 (s), 484 (s), 442 (w) cm^{-1}. Metathesis of [HBPMe][Cl] (6.03 g, 0.022 mol), purified as described above, with $AgSbF_6$ (8.11 g, 0.024 mol) in 200 mL of CH_3CN at room temperature for 16 h afforded a deep turquoise solution and a fine white precipitate of AgCl. The mixture was filtered. Flash evaporation of the solvent from the filtrate yielded a deep blue solution to which 100 mL of chlorobenzene was added. Further flash evaporation yielded golden microcrystals of [HBPMe][SbF_6], [**1**][SbF_6] (R_2 = H, R_1 = Me), which were collected by filtration, washed with chlorobenzene, and dried in vacuo, yield 7.42 g (0.015 mol, 72%). Recrystallization from glacial acetic acid afforded golden flakes, mp 240−242 °C. ^1H NMR (δ, CD_3CN): 7.69 (s, 1H, CH), 3.61 (s, 3H, N*Me*). IR: 1537 (vw), 1518 (m), 1492 (vs), 1360 (vs), 1149 (m), 1028 (s), 952 (w), 900 (w), 855 (m), 732 (vs), 667 (vs), 529 (m), 505 (w), 497 (vw), 474 (s) cm^{-1}. Anal. Calcd for $C_6H_4F_6N_3S_4Sb$: C, 14.95; H, 0.84; N, 8.72. Found: C, 15.20; H, 0.80; N, 8.58.

Preparation of 4-Ethyl-4*H*-bis[1,2,3]dithiazolo[4,5-*b*:5′,4′-*e*]pyridin-2-ium Hexafluoroantimonate [1][SbF_6] (R_2 = H, R_1 = Et). A solution of triethylamine (15.5 mL, 0.111 mol) in 15 mL of acetonitrile was added dropwise to a stirred solution of sulfur monochloride (7.4

mL, 0.093 mol) and **3** (R = Et, 5.32 g, 0.0185 mol) in 100 mL of acetonitrile at 0 °C. Once the addition was complete, the flask was sealed and left to stir at room temperature for 5 days. The resulting blue/black precipitate, crude [HBPEt][Cl], [**1**][Cl] (R_2 = H, R_1 = Et), was collected by filtration, washed with 100 mL of acetonitrile and 100 mL of dichloroethane, and then dried in vacuo, crude yield 8.59 g. Solid gallium trichloride (6.4 g, 0.036 mol) was added to a slurry of crude [HBPEt][Cl] (8.59 g, 0.029 mol) in 50 mL of acetonitrile and the deep green/blue solution so formed stirred for 30 m. A small amount of black insoluble material was filtered off, and the solvent was removed from the filtrate by flash distillation. The deep red microcrystalline solid [HBPEt][$GaCl_4$], [**1**][$GaCl_4$] (R_2 = H, R_1 = Et), so obtained was washed with 3 × 100 mL of acetic acid, collected by filtration and dried in vacuo, yield 4.53 g (9.61 mmol, 33%). The product was dissolved in 100 mL of acetonitrile, and to this was added 5 mL of pyridine to afford a dark purple precipitate of clean [HBPEt][Cl]. This purified powder was collected by filtration, washed with 2 × 50 mL of acetonitrile, and dried in vacuo, yield 2.59 g (8.76 mmol, 91% from [HBPEt][$GaCl_4$]), dec > 250 °C. IR: 1534 (w), 1482 (s), 1356 (s), 1326 (m), 1170 (vw), 1149 (w), 1041 (m), 878 (vw), 853 (vw), 788 (vw), 761 (vw), 737 (m), 728 (s), 649 (w), 548 (vw), 501 (s), 485 (s), 456 (w) cm^{-1}. Metathesis of [HBPEt][Cl] (2.92 g, 8.76 mmol), purified as described above, with $AgSbF_6$ (3.71 g, 10.8 mmol) in 100 mL of CH_3CN at room temperature for 16 h afforded a deep turquoise solution and a fine white precipitate of AgCl. The mixture was filtered. Flash evaporation of the solvent from the filtrate yielded a deep blue solution to which 100 mL of chlorobenzene was added. Further flash evaporation yielded golden microcrystals of [HBPMe][SbF_6], [**1**][SbF_6] (R_2 = H, R_1 = Et), which were collected by filtration, washed with chlorobenzene, and dried in vacuo, yield 3.33 g (6.71 mmol, 77%). Recrystallization from glacial acetic acid afforded golden flakes, mp 215−217 °C. ^{1}H NMR (δ, CD_3CN): 7.69 (s, 1H, CH), 4.15 (q, 2H, N$CH_2$$CH_3$, J = 7.12 Hz), 1.28 (t, 3H, NC$H_2$$CH_3$, J = 7.11 Hz). IR: 1489 (vs), 1168 (w), 1152 (m), 1090 (vw), 1045 (s), 997 (vw), 904 (w), 853 (w), 796 (m), 730 (vs), 660 (vs), 566 (vw), 505 (w), 472 (m) cm^{-1}. Anal. Calcd for $C_7H_6F_6N_3S_4Sb$: C, 16.95; H, 1.22; N, 8.47. Found: C, 17.11; H, 1.02; N, 8.35.

Preparation of 4*H*-Bis[1,2,3]dithiazolo[4,5-*b*:5′,4′-*e*]pyridin-2-ium Hexafluoroantimonate [1][SbF_6] (R_2 = R_1 = H). A solution of sulfur monochloride (13.0 mL, 163 mmol) in 50 mL of dichloroethane was added dropwise to a stirred solution of **4** (12.9 g, 32.5 mmol) in 300 mL of dichloroethane at 0 °C. The green solution and subsequent heavy black precipitate were left to stir overnight at room temperature. The precipitate was collected by filtration, washed with 3 × 200 mL of dichloroethane, and dried in vacuo to afford crude [HBPH][Cl], [**1**]-[Cl] (R_2 = R_1 = H), yield 8.35 g. The product was added to a solution of gallium trichloride (7.14 g, 40.5 mmol) in 100 mL of acetonitrile and the deep green/blue solution so formed stirred for 30 min. A small amount of black insoluble material was filtered off and the solvent removed from the filtrate by flash distillation. The deep red solid residue [HBPH][$GaCl_4$], [**1**][SbF_6] (R_2 = R_1 = H), so obtained was washed with 3 × 100 mL of acetic acid, collected by filtration, and dried in vacuo; yield 6.95 g (15.7 mmol, 50%). The product was dissolved in 100 mL of acetonitrile, and to this was added 5 mL of pyridine to afford a dark purple precipitate of purified [HBPH][Cl]. The fine powder was collected by filtration, washed with 2 × 50 mL of acetonitrile, and dried in vacuo, yield 4.10 g (15.3 mmol, 98% from [HBPH]-[$GaCl_4$]), dec > 200 °C. IR: 1592 (w), 1502 (w), 1346 (s), 1040 (m), 1032 (m), 723 (s), 630 (m), 494 (m) cm^{-1}. Metathesis of [HBPH][Cl] (4.10 g, 15.3 mmol), purified as described above, with $AgSbF_6$ (6.20 g, 18.0 mmol) in 100 mL CH_3CN at reflux for 16 h afforded a deep turquoise solution and a fine white precipitate of AgCl. The mixture was filtered and the solvent flash evaporated from the filtrate to yield a deep blue solution to which 100 mL of chlorobenzene was added. Further flash evaporation yielded golden microcrystals of [HBPH]-[SbF_6], [**1**][SbF_6] (R_2 = R_1 = H), which were collected by filtration, washed with chlorobenzene, and dried in vacuo, yield 6.4 g (13.8 mmol, 89%). Recrystallization from glacial acetic acid provided golden plates, dec > 220 °C. ^{1}H NMR (δ, CD_3CN): 7.64 (s, CH). IR: 1348 (s), 1034 (s), 728 (s), 659 (s), 636 (m), 486 (m) cm^{-1}. Anal. Calcd for $C_5H_2F_6N_3S_4Sb$: C, 12.83; H, 0.43; N, 8.98. Found: C, 13.12; H, 0.34; N, 8.94.

Preparation of 4-Methyl-4*H*-bis[1,2,3]dithiazolo[4,5-*b*:5′,4′-*e*]pyridin-3-yl HBPMe, 1 (R_2 = H, R_1 = Me). Solid decamethylferrocene (0.634 g, 1.94 mmol) was added to a solution of [**1**][SbF_6] (R_2 = H, R_1 = Me) (0.943 g, 1.95 mmol) in 15 mL of degassed (five freeze−pump−thaw cycles) acetonitrile and the resulting slurry stirred for 3 h at room temperature. Green/brown microcrystals of HBPMe **1** (R_2 = H, R_1 = Me) were collected by filtration, washed with 3 × 15 mL of acetonitrile, and dried in vacuo, yield 0.425 g (1.72 mmol, 89%). Recrystallization from hot, degassed (five freeze−pump−thaw cycles) toluene afforded green/bronze needles. IR: 1284 (w), 1205 (m), 1009 (m), 938 (w), 859 (w), 727 (s), 706 (s), 688 (s), 650 (m), 522 (m), 471 (m), 461 (w) cm^{-1}. Anal. Calcd for $C_6H_4N_3S_4$: C, 29.25; H, 1.64; N, 17.06. Found: C, 29.46; H, 1.42; N, 17.18.

Preparation of 4-Ethyl-4*H*-bis[1,2,3]dithiazolo[4,5-*b*:5′,4′-*e*]pyridin-3-yl HBPEt, 1 (R_2 = H, R_1 = Et). Solid decamethylferrocene (0.995 g, 3.05 mmol) was added to a solution of [**1**][SbF_6] (R_2 = H, R_1 = Et) (1.51 g, 3.05 mmol) in 15 mL of degassed (five freeze−pump−thaw cycles) acetonitrile and the resulting slurry stirred for 1 h at 70 °C. Green/brown microcrystals of HBPEt **1** (R_2 = H, R_1 = Et) were collected by filtration, washed with 3 × 15 mL of acetonitrile, and dried in vacuo, yield 0.670 g (2.57 mmol, 84%). Recrystallization from hot, degassed (five freeze−pump−thaw cycles) dichloroethane afforded green/bronze needles. IR: 1322 (m), 1247 (w), 1196 (s), 1029 (w), 833 (w), 728 (m), 709 (s), 690 (m), 645 (w), 545 (w), 473 (m), 455 (m) cm^{-1}. Anal. Calcd for $C_7H_6N_3S_4$: C, 32.29; H, 2.32; N, 16.14. Found: C, 32.37; H, 2.10; N, 16.30.

EPR Spectra. X-Band EPR spectra were recorded at ambient temperature using a Bruker EMX-200 spectrometer; samples of the radicals were dissolved in degassed dichloromethane. Hyperfine coupling constants were obtained by spectral simulation using Simfonia[28] and WinSim.

Electronic Stucture Calculations. Model density functional theory calculations on HBPH (anion, radical, and cation) were run on PC workstations using the B3LYP DFT method, as contained in the Gaussian 98W suite of programs.[29] Adiabatic (ΔSCF) ionization potential and electron affinity estimates were obtained from total electronic energy calculations using a 6-31G** basis set within the constraints of C_{2v} symmetry. Full vibrational frequency calculations on the final geometries of the radical and cation confirmed that they were stationary points. In the case of the anion, there was one negative frequency, which may be interpreted in terms of an incipient cleavage of one of the S−N bonds. Band electronic structure calculations were performed with the EHMACC suite of programs[30] using the Coulomb parameters of Basch, Viste, and Gray[31] and a quasi-split valence basis set adapted from Clementi and Roetti;[32] numerical values are tabulated elsewhere.[33] The off-diagonal elements of the Hamiltonian matrix were

(28) WinEPR Simfonia, Bruker Instruments, Inc., Billerica, MA.
(29) Gaussian 98, Revision A6: Frisch, M. J.; Trucks, G. W.; Schlegel, H. B.; Scuseria, G. E.; Robb, M. A.; Cheeseman, J. R.; Zakrzewski, V. G.; Montgomery, J. A., Jr.; Stratmann, R. E.; Burant, J. C.; Dapprich, S.; Millam, J. M.; Daniels, A. D.; Kudin, K. N.; Strain, M. C.; Farkas, O.; Tomasi, J.; Barons, V.; Cossi, M.; Cammi, R.; Mennucci, B.; Pomelli, C.; Adamo, C.; Clifford, S.; Ochterski, J.; Petersson, G. A.; Ayala, P. Y.; Cui, Q.; Morokuma, K.; Malick, D. K.; Rabuck, A. D.; Raghavachari, K.; Foreman, J. B.; Cioslowski, J.; Ortiz, J. V.; Stefanov, B. B.; Liu, G.; Fox, D. J.; Keith, T.; Al-Laham, M. A.; Peng, C. Y.; Nanayakkara, A.; Wong, M. W.; Andres, J. L.; Gonzalez, C.; Head-Gordon, M.; Repogle, E. S.; Pople, J. A. Gaussian, Inc., Pittsburgh, PA, 1998.
(30) EHMACC, Quantum Chemistry Program Exchange, program number 571.
(31) Basch, H.; Viste, A.; Gray, H. B. *Theor. Chim. Acta* **1965**, *3*, 458.
(32) Clementi, E.; Roetti, C. *At. Data. Nucl. Data Tables* **1974**, *14*, 177.
(33) Cordes, A. W.; Haddon, R. C.; Oakley, R. T.; Schneemeyer, L. F.; Waszczak, J. V.; Young, K. M.; Zimmerman, N. M. *J. Am. Chem. Soc.* **1991**, *113*, 582.

calculated with the standard weighting formula.[34] Atomic positions were taken from the crystallographic data. In the bandwidth vs slippage calculations a rigorously planar HBPH ring was used, with coordinates taken from a B3LYP/6-31G** calculation.

Cyclic Voltammetry. Cyclic voltammetry was performed using a PINE Bipotentiostat, Model AFCClBP1, with scan rates of 50−100 mV s^{-1} on solutions ($<10^{-3}$ M) of [HBPMe][SbF_6] and [HBPEt][SbF_6] in CH_3CN (dried by distillation from P_2O_5) containing 0.1 M tetra-*n*-butylammonium hexafluorophosphate. Potentials were scanned with respect to the quasi-reference electrode in a single compartment cell fitted with Pt electrodes and referenced to the Fc/Fc^+ couple of ferrocene at 0.38 V vs SCE.[35] The $E_{pa} - E_{pc}$ separation of the reversible couples were within 10% of that of the Fc/Fc^+ couple.

X-ray Measurements. A sample of HBPEt was glued to a glass fiber, centered on a Bruker P4/CCD diffractometer, and irradiated using 11.25 kW X-rays from a Bruker Mo rotating anode generator. The data were scanned using Bruker's SMART[36] program and integrated using Bruker's SAINT[37] software. Data collection details on HBPMe were reported earlier.[12]

Magnetic Susceptibility Measurements. Magnetic susceptibilities were measured over the temperature range 5−380 K on a George Associates Faraday balance operating at 0.5 T.

Conductivity Measurements. Single-crystal (along the needle axis) conductivities were measured in a four-probe configuration, with in-line contacts made using silver paint. Conductivity was measured in a custom-made helium variable-temperature probe using a Lake Shore 340 temperature controller. A Keithley 236 unit was used as a voltage source and current meter, and two 6517A Keithley electrometers were used to measure the voltage drop between the potential leads in the four-probe configuration.

Near-Infrared Measurements. The transmission spectrum of a single crystal of HBPEt was measured using a Continuum Thermo-Nicolet FTIR microscope integrated with a Nexus-670 FTIR Nicolet spectrometer.

Acknowledgment. We thank the Natural Sciences and Engineering Research Council of Canada (NSERCC), the U.S. Office of Basic Energy Sciences, Department of Energy (Grant No. DE-FG02-97ER45668), the Office of Naval Research (Contract No. N00014-99-1-0392), and the Arkansas Science and Technology Authority for financial support. We also thank the NSERCC for a post-graduate scholarship to L.B.

Supporting Information Available: Details of X-ray crystallographic data collection and structure refinement, tables of atomic coordinates, bond distances and angles, anisotropic thermal parameters and hydrogen atom positions for HBPEt (CIF). This material is available free of charge via the Internet at http://pubs.acs.org.

JA0371350

(34) Ammeter, J. H.; Bürgi, H. B.; Thibeault, J. C.; Hoffmann, R. *J. Am. Chem. Soc.* **1978**, *100*, 3686.
(35) Boeré, R. T.; Moock, K. H.; Parvez, M. *Z. Anorg. Allg. Chem.* **1994**, *620*, 1589.
(36) SMART, Version 4.05, Bruker AXS Inc. Madison, WI , 1996.
(37) SAINT, Version 4.05, Bruker AXS Inc. Madison, WI, 1996.